Journal of Inorganic Biochemistry 260 (2024) 112695

Contents lists available at ScienceDirect

Journal of Inorganic Biochemistry

journal homepage: www.elsevier.com/locate/jinorgbio

Endoplasmic reticulum-targeted iridium(III) photosensitizer induces pyroptosis for augmented tumor immunotherapy

Yun-Shi Zhi [a,b,1], Tie Chen [b,1], Bin-Fa Liang [b], Shan Jiang [a], Da-Hong Yao [a], Zhen-Dan He [a], Chen-Yang Li [b,*], Liang He [c,*], Zheng-Yin Pan [a,*]

[a] College of Pharmacy, Shenzhen Technology University, Shenzhen 518118, China.
[b] School of Pharmacy, Shenzhen University Medical School, Shenzhen University, Shenzhen 518055, China
[c] Key Laboratory for Biobased Materials and Energy of Ministry of Education, College of Materials and Energy, South China Agricultural University, Guangzhou 510642, China

ARTICLE INFO

Keywords:
Iridium(III) complex
Photodynamic therapy
Immunotherapy
Pyroptosis
Endoplasmic reticulum
Antitumor

ABSTRACT

An ideal tumor treatment strategy involves therapeutic approaches that can enhance the immunogenicity of the tumor microenvironment while simultaneously eliminating the primary tumor. A cholic acid-modified iridium (III) (**Ir3**) photosensitizer, targeted to the endoplasmic reticulum (ER), has been reported to exhibit potent type I and type II photodynamic therapeutic effects against triple-negative breast cancer (MDA-MB-231). This photosensitizer induces pyroptotic cell death mediated by gasdermin E (GSDME) through photodynamic means and enhances tumor immunotherapy. Mechanistic studies have revealed that complex **Ir3** induces characteristics of damage-related molecular patterns (DAMPs) in MDA-MB-231 breast cancer cells under light conditions. These include cell-surface calreticulin (CRT) eversion, extracellular high mobility group box 1 (HMGB1) and ATP release, accompanied by ER stress and increased reactive oxygen species (ROS). Consequently, complex **Ir3** promotes dendritic cell maturation and antigen presentation under light conditions, fully activates T cell-dependent immune response *in vivo*, and ultimately eliminates distant tumors while destroying primary tumors. In conclusion, immune regulation and targeted intervention mediated by metal complexes represent a new and promising approach to tumor therapy. This provides an effective strategy for the development of combined targeted therapy and immunotherapy.

1. Introduction

Tumor immunology is an emerging field of "personalized" medicine. It is an antitumor response that strengthens the immune system to attack immune molecules overexpressed by tumor cells or expressed only by tumor cells [1]. Many biomolecular or small molecule drugs are used to rebalance the tumor immune response to kill tumors [2]. Immune checkpoint inhibitors (ICBs) therapies are highly successful in preventing tumor-mediated T cell inactivation. However, it is effective in only about 20% of patients and most patients do not achieve lasting benefit [3]. The tumor microenvironment (TME), especially the tumor immune microenvironment (TIME) lacking T cell inflammation, determines the effectiveness of tumor immunotherapy [4–6].

Numerous studies have shown that photodynamic therapy (PDT) can cause tumor cell death in an immunogenic manner. Furthermore, PDT is a non-invasive treatment and has been extensively studied in the treatment of localized cancers [7–9]. Under laser irradiation focused on localized tumors, photosensitizers (PSs) rapidly generate cytotoxic

Abbreviations: ER, Endoplasmic reticulum; CA, Cholic acid; GSDME, Gasdermin E; DAMPs, Damage-related molecular patterns; CRT, Calreticulin; HMGB1, High mobility group box 1; ROS, Reactive oxygen species; ICBs, Immune checkpoint inhibitors; TME, Microenvironment; PDT, Photodynamic therapy; PS, Photosensitizer; ICD, Immunogenic cell death; GSDMD, Gasdermin D; LAP, Leucine aminopeptidase; MLCT, Metal-ligand charge transfer; ABDA, 9,10-anthracenediyl-bis(methylene) dimalonic acid; PCC, Pearson colocalization coefficient; MTT, 3-(4,5-dimethylthiazol-2-yl)-2,5-diphenyltetrazolium bromide; IC_{50}, Half maximal inhibitory concentration; PI, Phototoxicity index; DCFH-DA, 2′,7′-dichlorodihydrofluorescein diacetate; ERS, ER stress; UPR, Unfolded protein response; ATF4, Activating transcription factor 4; CHOP, C/EBP-homologous protein; STAT3, Signal transducer and activator of transcription 3; DCs, Dendritic cells; H&E, Hematoxylin and eosin.

* Corresponding authors.
E-mail addresses: lcy@szu.edu.cn (C.-Y. Li), heliang@scau.edu.cn (L. He), panzhengyin@sztu.edu.cn (Z.-Y. Pan).
[1] These authors made equal contributions to this work.

https://doi.org/10.1016/j.jinorgbio.2024.112695
Received 9 June 2024; Received in revised form 17 July 2024; Accepted 10 August 2024
Available online 11 August 2024

reactive oxygen species (ROS) and selectively damage diseased tissues [10]. In addition, ROS produced by PSs can not only promote tumor cell death, but also trigger endoplasmic reticulum (ER) stress and trigger cell-surface calreticulin (CRT) protein exposure, thereby inducing immunogenic cell death (ICD) of cancer cells and releasing damage-related molecular patterns (DAMPs) and pro-inflammatory cytokines [11,12].

ER is an indispensable organelle responsible for protein synthesis, intracellular signal transduction, and calcium homeostasis, and plays a vital role in the immune system [13]. In addition, subtle disturbances to the ER redox signaling pathway are likely to lead to ER stress, which induces ICD [12,14]. Recently, Chao's groups reported that ER-targeting metal iridium complexes combined with PDT can enhance ICD[15].

Pyroptosis is a new type of programmed cell death different from apoptosis, which can cause a strong inflammatory response. It has the potential to stimulate antitumor immunity, eliminate primary tumors, and inhibit tumor metastasis [16]. Activating Caspase-1/11/4/5 can cut Gasdermin D (GSDMD) to form GSDMD-N-terminus (GSDMD-NT) and GSDMD-C-terminus (GSDMD-CT). GSDMD-CT "oligomerizes" to form membrane pores and induce pyroptosis [17]. In addition, activated Caspase-3 can also lyse GSDME to form GSDME-NT and GSDME-CT, which manifests as pyroptosis [18]. This pathway also activates the inflammatory response by perforating the cell membrane and releasing the cell contents outward [19]. Overexpression of GSDME has been shown to promote tumor sensitivity of small molecule-targeted inhibitors [20]. Pyroptosis can trigger ICD and convert "cold" immunosuppressive TME into "hot" immunogenic TME with extensive tumor lymphocyte infiltration [21].

Due to the great clinical success of traditional platinum-based drugs, researchers have also begun to focus on other metal drugs, such as cyclometalated iridium(III) complexes [22–25]. Cyclometalated iridium (III) complexes have superior photophysical properties and anti-cancer efficacy, which is helpful to study their localization and anti-cancer mechanism in cells, so as to develop new anti-cancer drugs with diagnostic and therapeutic functions [26–28]. ROS produced by PDT has a certain killing range [29]. Organelle localization of photosensitizers is closely related to therapeutic effect. Therefore, it is of great significance to find photosensitizers with organelle-targeting functions [30,31].

Most imaging probes are easily removed quickly after entering the liver and are difficult to accumulate fully in the liver in a short period of time, resulting in low signal intensity and sensitivity in the liver [32]. Cholic acid, a signaling molecule that enters hepatocytes through "active transport", is involved in many hepatic metabolisms and exhibits inherent hepatocyte targeting [33,34]. Su's group designed hCy-CA-LAP, a leucine aminopeptidase (LAP)-activated fluorescent probe, which greatly improved the targeting ability of hepatocytes by introducing cholic acid groups, showing high selectivity, high sensitivity, and low detection limit (0.0067 U·mL^{-1}). It has successfully enabled imaging diagnostics of trace amounts of LAP *in vivo* [35]. In addition, Andriy Mokhir's group developed an ER-targeted conjugate, a prodrug of cholic acid and *N*-alkylaminoferrocene, which is specifically activated in cancer cells with elevated ROS levels [36]. The conjugate induced ER stress by accumulating in the ER of cancer cells, and further caused cell necrosis by reducing mitochondrial membrane potential and producing mitochondrial ROS.

Therefore, novel cyclometalated iridium(III) complexes **Ir1-Ir3** functionalized with cholic acid groups were designed and synthesized (Scheme 1), which have excellent singlet oxygen production capacity. All of these complexes showed photodynamic therapeutic activity against triple-negative breast cancer, with **Ir3** being the most active. Mechanistic studies have found that **Ir3** accumulates in the ER, which promotes the *in situ* production of ROS on the ER and triggers ER stress under visible light (425 nm) irradiation. **Ir3** exhibits excellent phototoxicity in nanomolar concentration against human triple-negative breast cancer cells MDA-MB-231 and mouse breast cancer 4T1 cells. It effectively initiates GSDME-mediated pyroptosis and triggers ICD.

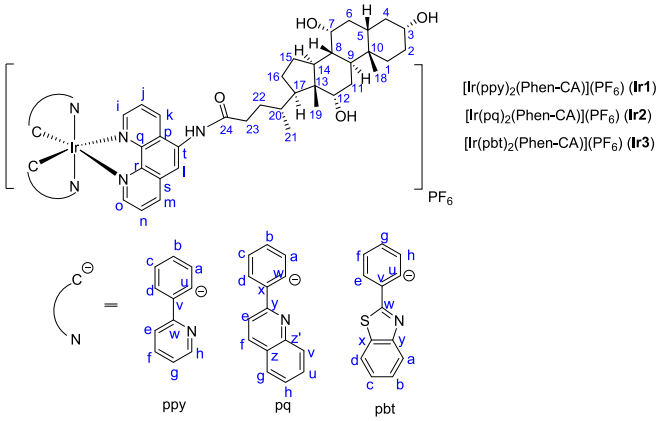

Scheme 1. Structures of **Ir1–Ir3**.

What's more, the antitumor immune-therapeutic effect of **Ir3** was verified in a mouse tumor model.

2. Results and discussion

2.1. Synthesis and characterization

The synthesis route of complexes **Ir1-Ir3** is shown in Scheme S1. Ligand **Phen-CA** was synthesized as previously reported [37]. The complexes **Ir1-Ir3** were synthesized by conventional methods [38]. The complexes **Ir1-Ir3** were characterized by ESI-MS (Fig. S1-S3), ^{1}H NMR (Fig. S4-S6), and ^{13}C NMR spectra (Fig. S7-S9). The mass spectrometry data and the result of the ^{1}H and ^{13}C NMR tentative assignments confirmed the composition of these complexes [39,40].

The UV–Vis absorption spectra of **Ir1-Ir3** exhibit a strong intraligand transition band at 250–315 nm, and two relatively weak broad bands at 315–365 and 365–460 nm attributed to the mixed metal-ligand charge transfer ([1]MLCT and [3]MLCT) (Fig. 1A and Fig. S10A-B) [41]. The strong absorption properties of the complexes in the visible region (400–480 nm) make it a potential visible excitation photosensitizer. Moreover, complexes **Ir1-Ir3** exhibit orange-red emission in the region of about 510–650 nm, which is attributed to the [3]MLCT excited state of the complexes (Fig. 1B and Fig. S10C-D).

The ability of **Ir1-Ir3** to generate singlet oxygen ($^{1}O_2$) was investigated by using 9,10-anthracenediyl-bis(methylene)dimalonic acid (ABDA) as a singlet oxygen ($^{1}O_2$) probe. In the presence of **Ir1-Ir3** and 425 nm light irradiation, the maximum absorption of ABDA at 380 nm gradually decreases, indicating that the $^{1}O_2$ is produced (Fig. 1C). Among the three complexes, **Ir2** and **Ir3** have higher singlet oxygen yields of 0.65 and 0.67, respectively, probably due to the larger conjugation properties of the ligands pq and pbt.

2.2. Cellular localization

Due to the intrinsic phosphorescent properties of **Ir3**, its suborganelle localization after entering cells can be explored by laser confocal fluorescence microscopy. Colocalization experiments were performed in MDA-MB-231 cells by co-staining **Ir3** with the probe of ER-Tracker Deep Red. As shown in Fig. 2, the fluorescence of **Ir3** (shown in green) in the cells overlaps to a large extent with the fluorescence of ER-Tracker Deep Red (shown in red), and the Pearson colocalization coefficient (PCC) value is 0.90, indicating that **Ir3** predominantly accumulates in the ER after entering the cells. Some other lipophilic cationic iridium complexes have also been reported in the literature to localize primarily to the ER [42,43]. Thus, **Ir3** acts as an ER-targeted PDT photosensitizer. The auxiliary ligand of iridium(III) complexes coupled with some hydrophobic molecules, such as bis(2-chloroethyl)-azane [15], *N*-phenethylsuccinamide [30], rhodamine [43], *etc.*, can

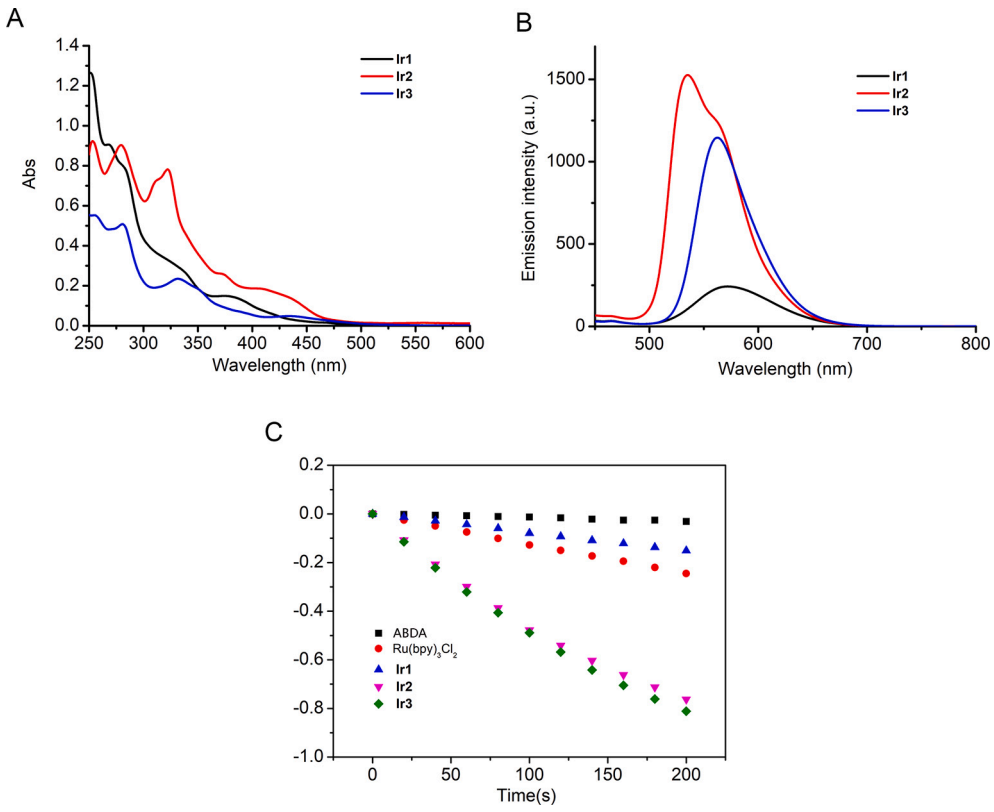

Fig. 1. (A) UV/Vis and (B) emission spectra of **Ir1–Ir3** (2×10^{-5} M) measured in CH_3CN at 298 K. (C) Changes in the absorption spectra of ABDA at 380 nm upon irradiation at 425 nm in the presence of **Ir1–Ir3** in aerated PBS. $[Ru(bpy)_3]Cl_2$ was used as a standard.

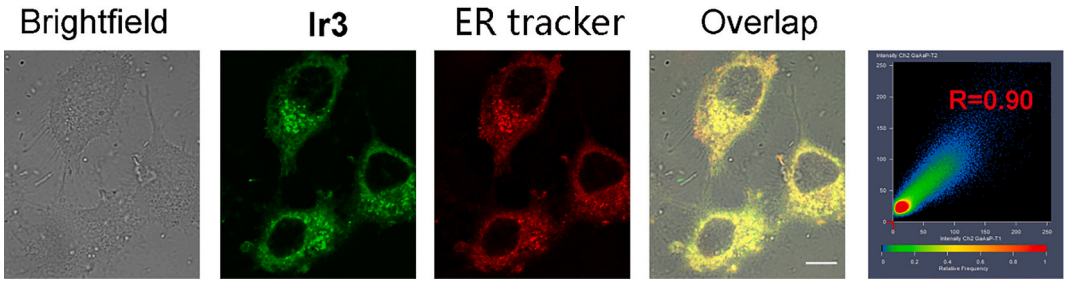

Fig. 2. Confocal co-localization images of MDA-MB-231 cells treated with **Ir3** (10 μM, 4 h; Ex = 405 nm, Em = 550–600 nm) and then stained with ER-Tracker Deep Red FM (150 nM, 30 min; Ex = 633 nm, Em = 660–700 nm). The scale bar represents 20 μm. (For interpretation of the references to colour in this figure legend, the reader is referred to the web version of this article.)

effectively target the endoplasmic reticulum. Andriy Mokhir's team reported that cholic acid-modified prodrugs of *N*-alkylaminoferrocene could well target the endoplasmic reticulum of cells [36]. In addition, the lipophilicity of **Ir3** also facilitates targeting the endoplasmic reticulum. Therefore, we believe that the endoplasmic reticulum targeting properties of **Ir3** may be related to the lipophilicity and the cholic acid group of the complex.

2.3. PDT activity

The photodynamic activity of **Ir1–Ir3** on MDA-MB-231 and 4T1 cells was detected by 3-(4,5-dimethylthiazol-2-yl)-2,5-diphenyltetrazolium bromide (MTT) colorimetric assay. As shown in Table 1, after 15 min irradiation with 425 nm laser (15 mW/cm^2), the half maximum inhibitory concentrations (IC_{50}) obtained for **Ir2** and **Ir3** on MDA-MB-231 were 0.010 μM and 0.009 μM, respectively, both down to the nanomolar level. Moreover, the IC_{50} values for 4T1 cells upon light irradiation were 0.18 μM and 0.34 μM, respectively, showing significant

Table 1
Antiproliferative activities (IC_{50}/μM) of the compounds in the absence and presence of 425 nm light in MDA-MB-231 and 4T1 cells.

Cell Lines	MDA-MB-231			4T1		
Condition	Dark[a]	Light[b]	PI[c]	Dark[a]	Light[b]	PI[c]
Ir1	6.8 ± 0.21	0.098 ± 0.1	69.0	10.2 ± 0.4	2.4 ± 0.3	4.3
Ir2	4.6 ± 0.13	0.01 ± 0.04	459.2	3.1 ± 0.14	0.18 ± 0.04	17.3
Ir3	7.6 ± 0.18	0.009 ± 0.02	838.9	8.3 ± 0.12	0.3 ± 0.03	24.6

a: Cells were incubated with the indicated compounds in the dark for 48 h.
b: Cells were incubated with the indicated compounds for 12 h in the dark and then irradiated with light at 425 nm.
c: PI = Phototoxicity Index, PI is the ratio of the IC_{50} values in the dark to those obtained upon light irradiation.

phototoxicity. Among these complexes, **Ir3** showed the highest phototoxicity index (PI) against MDA-MB-231 and 4T1, which were 838.89 and 24.63, respectively. These results show that **Ir3** exhibits excellent photodynamic therapeutic activity *in vitro*.

2.4. ROS generation

The therapeutic effect of PDT depends on the fact that cancer cells produce sufficient cytotoxic ROS. Therefore, we used 2′,7′-dichlorodihydrofluorescein diacetate (DCFH-DA) as a capture probe for ROS to detect the ability of **Ir3** to induce ROS production in MDA-MB-231 cells under light conditions. DCFH-DA is a non-fluorescent probe that can penetrate cell membranes. It is oxidized by the ROS inside the cell, resulting in highly fluorescent DCF. The results of laser confocal imaging showed that the intracellular fluorescence in the control group was weak, while under laser irradiation, the intracellular fluorescence in the **Ir3**-treated group gradually increased with the increase of **Ir3** concentration (Fig. 3A). Flow cytometry further validated **Ir3**'s ability to induce cells to produce ROS after laser irradiation (Fig. 3B). In summary, **Ir3** can effectively induce intracellular ROS production under laser irradiation.

It is well known that traditional type II PDT relies on the production of $^1O_2$, and this PDT mode is less effective in the treatment of hypoxic tumors, while the type I PDT that induces the production of superoxide anion radicals ($O_2^{\bullet-}$) has advantages in the treatment of hypoxic tumors due to its reduced dependence on oxygen [44]. We then used the superoxide anion ($O_2^{\bullet-}$) probe dihydroethidium to detect the production of $O_2^{\bullet-}$. By confocal microscopy imaging (Fig. 3C), it can be seen that after PDT treatment, as the **Ir3** concentration (0 μM, 0.1 μM, 0.2 μM, and 0.4 μM) increases, the $O_2^{\bullet-}$ produced in MDA-MB-231 cells also increase. These results indicate that both type I and type II PDT are involved in the mechanism of **Ir3**-induced cell death.

2.5. Analysis of the expression of intracellular endoplasmic reticulum-associated proteins

External stimuli can cause an increase in unfolded and misfolded proteins within the ER, and cause ER stress (ERS), which further rapidly activates unfolded protein response (UPR) signals in response [28–30]. Under ERS, PERK auto-phosphorylation and subsequent phosphorylation of eIF2α restore cellular homeostasis. However, persistent ERS promotes the expression of activating transcription factor 4 (ATF4) [45]. ATF4 is involved in processes such as cell metabolism, nutrient uptake, and antioxidant. ATF6 is a type 2 transmembrane protein in the ER. In ERS, ATF6 promotes transcription of UPR-associated genes to eliminate misfolded proteins, allowing cells to survive under ERS [46,47]. However, under long-term ERS, ATF4 and ATF6 can activate downstream proteins such as C/EBP-homologous protein (CHOP), thereby inducing apoptosis [48].

In summary, when UPR cannot alleviate ERS, many pro-apoptotic signaling pathways, such as CHOP up-regulation, are initiated. After MDA-MB-231 cells were stimulated by **Ir3** and laser, a large amount of ROS was accumulated in the ER, which increased the pressure on the ER. Compared with the control group, the expression of PERK and ATF6 proteins decreased and the expression of ATF4 and CHOP proteins increased significantly with the increase of **Ir3** concentration in MDA-MB-231 cells treated with **Ir3** and laser (Fig. 4). The above results indicate that **Ir3** damages the ER and cause tumor cell death.

Signal transducer and activator of transcription 3 (STAT3) is the key molecule in many oncogenic signaling pathways that can induce epithelial-mesenchymal transformation and promote apoptosis [49]. Studies have pointed out that inhibition of p-STAT3 can promote the expression of CHOP [50]. In addition, STAT3 promotes communication between tumors and individual immune cell subsets, impeding tumor transformation from "cold" to "hot" [51]. Therefore, **Ir3** is targeted to the ER, and after laser stimulation, the expression of intracellular p-STAT3 decreases significantly with dose dependence, which facilitates the transformation of "cold" tumors to "hot" tumors and initiates CHOP-mediated ERS.

2.6. Pyroptosis induction

Ir3-induced cell death pattern under PDT treatment was studied through a variety of experiments. Firstly, it was observed by inverted microscopy and transmission electron microscopy that the cells in the control group treated by light alone had normal growth, good elongation, and normal morphology. In the **Ir3** plus PDT group, the cells were rounded and swollen, the intercellular space was significantly enlarged, the cell morphology and contour were unclear, and the volume and density were significantly reduced. In addition, there are many distinct vacuoles released on the cell membrane surface (Fig. 5A and B). These morphological changes are typical of pyroptosis.

Furthermore, Western blot analysis was used to detect catalytic cleavage of GSDME, which is considered one of the important indicators of pyroptosis. As shown in Fig. 5C, the expression of cleaved caspase-3 and GSDME-N in **Ir3**-treated cells increased significantly with laser time-dependence. These results suggest that **Ir3**-mediated PDT induces cells to activate cleaved caspase-3 and cleaved GSDME (GSDME-N), perforating cell membranes and triggering pyroptosis to kill cancer cells.

2.7. Tumor immunogenic cell death induction

PDT-induced pyroptosis may cause immunogenic cell death (ICD). ICD has three distinct biochemical signatures of DAMPs: HMGB1 release, etco-CRT exposure, and ATP exosomes. To investigate whether PDT treatment with **Ir3** triggers ICD, we first observed changes in intracellular etco-CRT and HMGB1 expression upon 425 nm laser irradiation after **Ir3** (0 μM, 0.1 μM, 0.2 μM, and 0.4 μM) treatment. Immunofluorescence imaging was shown in Fig. 6A. The red fluorescence (ecto-CRT) in the cells of the control group was negligible under dark conditions, but the red fluorescence in the cells of the **Ir3** group was significantly enhanced by 425 nm laser irradiation (15 mW/cm^2, 15 min), indicating high expression of ecto-CRT in cells after treatment by **Ir3** and PDT. In addition, quantitative analysis of the above results using flow cytometry (Fig. 6B) showed a concentration-dependent increase in intracellular immunofluorescence intensity after treatment with **Ir3** and PDT.

At the same time, as shown in Fig. 6C, with the increase of **Ir3** concentration, the green fluorescence (HMGB1) inside cells gradually decreases under laser irradiation, indicating that HMGB1 migrates from the nucleus to the cytoplasm and exosomes to the extracellular. Next, we tested the change in extracellular ATP content after treatment with **Ir3** (0 μM, 0.1 μM, 0.2 μM, and 0.4 μM) under light and dark conditions (Fig. 6D). ATP in the extracellular supernatant of cells treated with **Ir3** (0.4 μM) and PDT was significantly increased compared to the control group. In summary, cells treated by **Ir3** and PDT have high immunogenicity and excellent anti-tumor immunity potential.

2.8. In vivo anti-tumor evaluation

To investigate the antitumor efficacy and systemic immune response of **Ir3**-mediated PDT *in vivo*, we chose to construct a BALB/C mouse model of 4T1 tumors instead of human triple-negative breast cancer MDA-MB-231 tumors. Mice were implanted with primary tumors on the right side. After 7 days, when the volume of the primary tumor reached 50–100 mm^3, mice were implanted with the distal tumor on the left side. After 1 day, mice were randomly divided into 4 groups. 5 mg/kg **Ir3** was administered within the primary tumor, followed by 425 nm PDT treatment. Distal tumors were left untreated to observe the immune response. Among them, Ctrl + dark group, Ctrl + light group, and **Ir3** group were used as controls.

As shown in Fig. S11, **Ir3** has a good inhibitory effect on 4T1 tumor

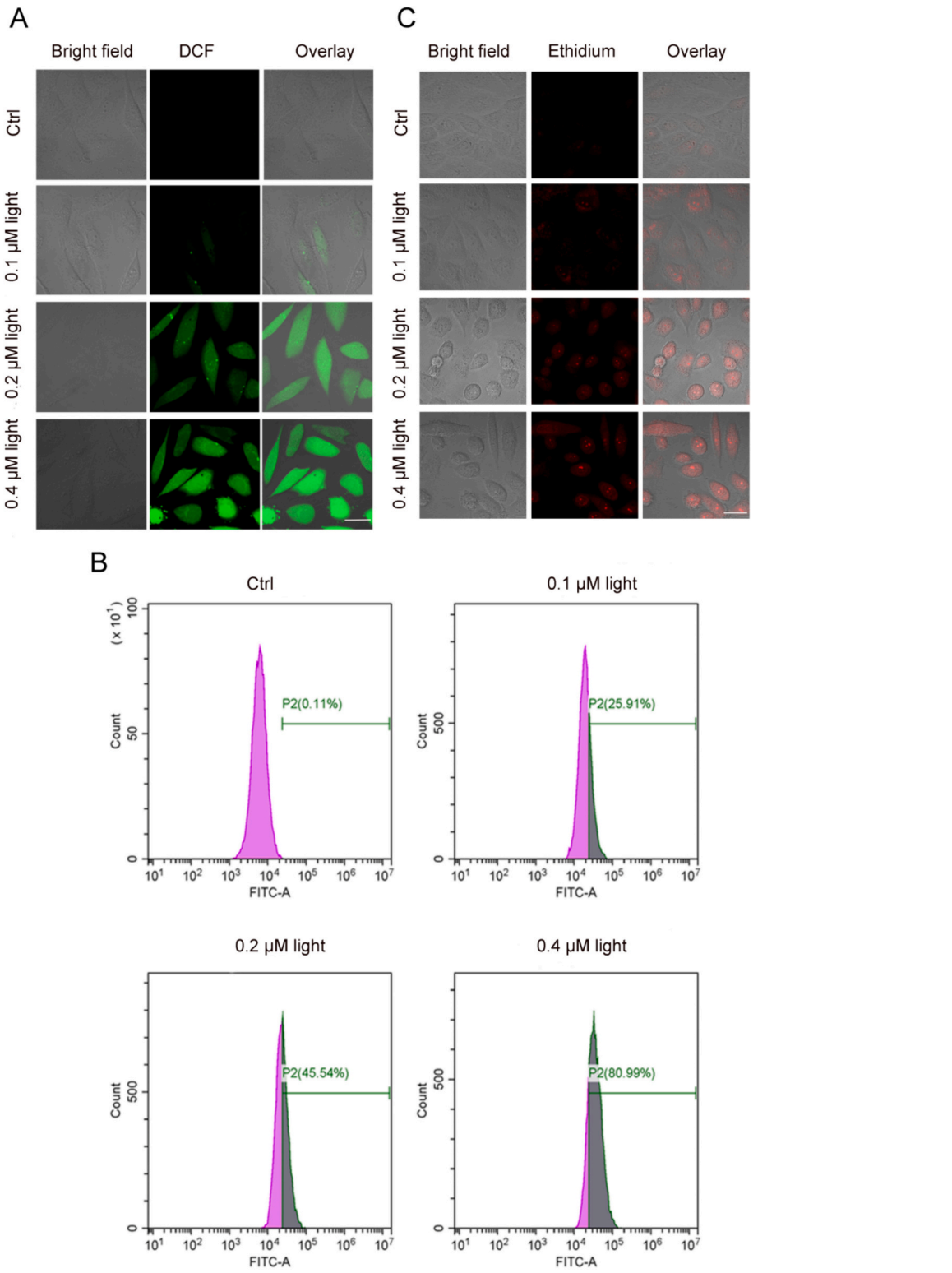

Fig. 3. Detection of cellular ROS levels in MDA-MB-231 cells by (A) confocal microscopy and (B) flow cytometry. Cells were treated with **Ir3** (0.1, 0.2, 0.4 μM) for 12 h and stained with DCFH-DA (10 μM) for 20 min. Cells were then irradiated with a green LED light (λ_{ir} = 425 nm, 15 mW/cm^2) for 15 min. Ex = 488 nm, Em = 520 ± 20 nm. Scale bar, 20 μm. (C) Detection of the production of $O_2^{\bullet-}$ in MDA-MB-231 cells by flow cytometry after **Ir3** and PDT treatment. Scale bar: 20 μm. Dihydroethidium: E_x = 561 nm, E_m = 620 ± 20 nm. (For interpretation of the references to colour in this figure legend, the reader is referred to the web version of this article.)

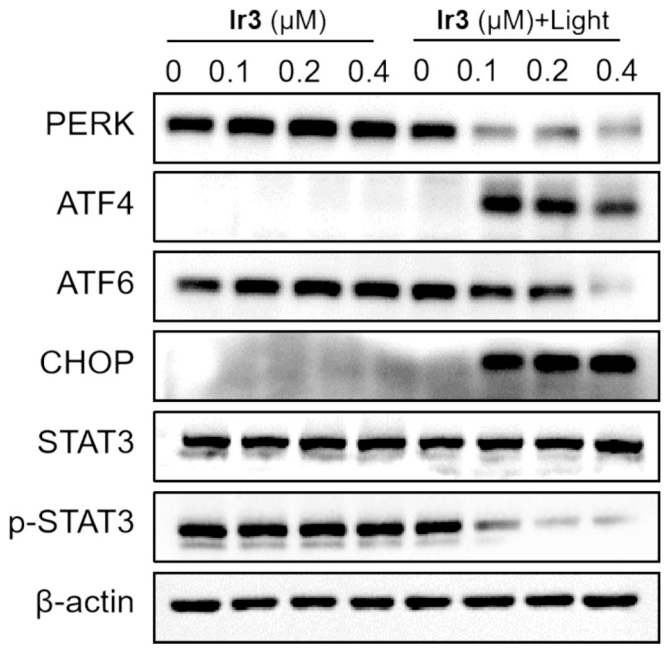

Fig. 4. Expression of STAT3, p-STAT3, ATF6, PERK, ATF4 and CHOP proteins. MDA-MB-231 cells were treated with **Ir3** (1 μM, 4 h), irradiated with 425 nm light for indicated time intervals, and further incubated for 4 h.

growth under light (425 nm) irradiation. On the end day of PDT treatment (day 16), tumor volume was suppressed by approximately 86% in mice treated with **Ir3** and PDT (Fig. 7A and B). At the same time, we assessed the immune effect of distal tumors in each group by measuring the growth rate of distal tumors under dark conditions. There were no significant suppressive effects on distal tumors in the Ctrl + light group, Ctrl + dark group, and **Ir3** group. Their distant tumors were enlarged to about 402.82 mm^3, 412.82 mm^3, and 249.65 mm^3, respectively. The growth rate of distal tumors in the **Ir3** + light group was significantly inhibited compared with the control group. The inhibition rate of distal tumors in the **Ir3** + light group was as high as about 83%, and its size only increased to about 68.68 mm^3. These results showed that **Ir3** could effectively inhibit distant tumors after PDT treatment, indicating that **Ir3** had excellent anti-tumor immune effects.

Tumor-infiltrated immune cells were analyzed by flow cytometry to assess the anti-tumor immune response of mice. Firstly, we assessed the degree of maturation of dendritic cells (DCs) in the lymph nodes of tumors, which is necessary for anti-tumor immunity. As shown in Fig. 7C, $CD80^+$ $CD86^+$ dendritic cells in the **Ir3** + light group increased significantly from 7.83% to 23.6% compared with the Ctrl + light group, Ctrl + dark group, and **Ir3** group, indicating that the maturity of DCs increased after **Ir3** and PDT treatment. Secondly, we quantified $CD8^+$ cytotoxic T cells and $CD4^+$ helper T cells which are indicators of adaptive immune responses in distant tumors. The proportion of tumor-infiltrated $CD3^+$ $CD4^+$ and $CD3^+$ $CD8^+$ T lymphocytes in the **Ir3** + light group were 36.3% and 21.7%, respectively, which were 3–7 times higher than those in the Ctrl + dark group (11% and 3.76%), the Ctrl + light group (0.6% and 5.76%) and the **Ir3** group (14.3% and 6.34%) (Fig. 7D and E). In summary, cytotoxic T lymphocytes can be induced by **Ir3** and PDT to activate adaptive anticancer immune responses.

During **Ir3** and PDT treatment in mice, toxic and side effects of the **Ir3** + light group were evaluated. The body weight of BALB/C mice loaded with 4T1 tumors remained stable, and no mice died or lost weight significantly (Fig. S12). Hematoxylin and eosin (H&E) staining showed that no significant pathological abnormalities were found in the major organs (heart, kidney, liver, spleen and lung) of **Ir3** + group (Fig. S13). In summary, it shows that **Ir3** has very low systemic toxicity and side effects *in vivo* after PDT treatment.

3. Conclusions

We have developed a novel iridium(III) photosensitizer **Ir3** that targets the ER and can induce pyroptosis, which can effectively activate the anti-tumor immune response *in vivo*. **Ir3** shows nanomolar phototoxicity (Light IC_{50} = 9 nM), and the phototoxicity index for MDA-MB-231 reaches 838.9. Under visible light (425 nm) irradiation, singlet oxygen can be effectively generated, and it has high photostability. Mechanistic studies have shown that **Ir3** causes excessive ROS production and ERS in MDA-MB-231 cells under light irradiation. Interestingly, **Ir3** can cause GSDME-mediated pyroptosis to enhance tumor immunogenicity. **Ir3** promotes dendritic cell maturation and activates T cell-dependent adaptive immune responses in mice. Ultimately, **Ir3** eliminates the distant tumor while destroying the primary tumor. In summary, the results suggest that **Ir3** is a novel photosensitizer that targets

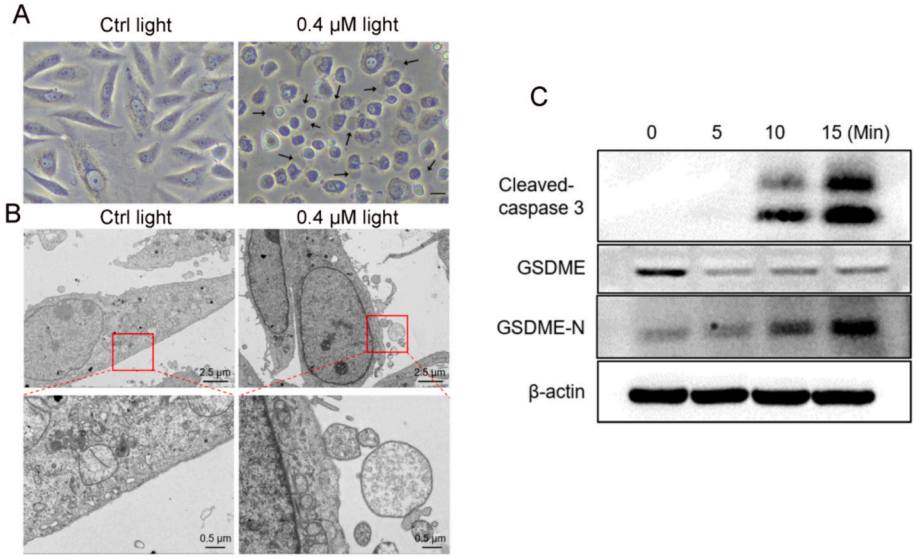

Fig. 5. (A) Inverted microscope and (B) transmission electron microscope images of MDA-MB-231 cells treated with **Ir3** (0.4 μM) and PDT. Black arrows indicate areas where cellular vacuoles are released. Scale bar: 20 μm. (C) Expression of cleaved-caspase 3, GSDME, and GSDME-N proteins in MDA-MB-231 cells treated with **Ir3** (0.4 μM) and PDT.

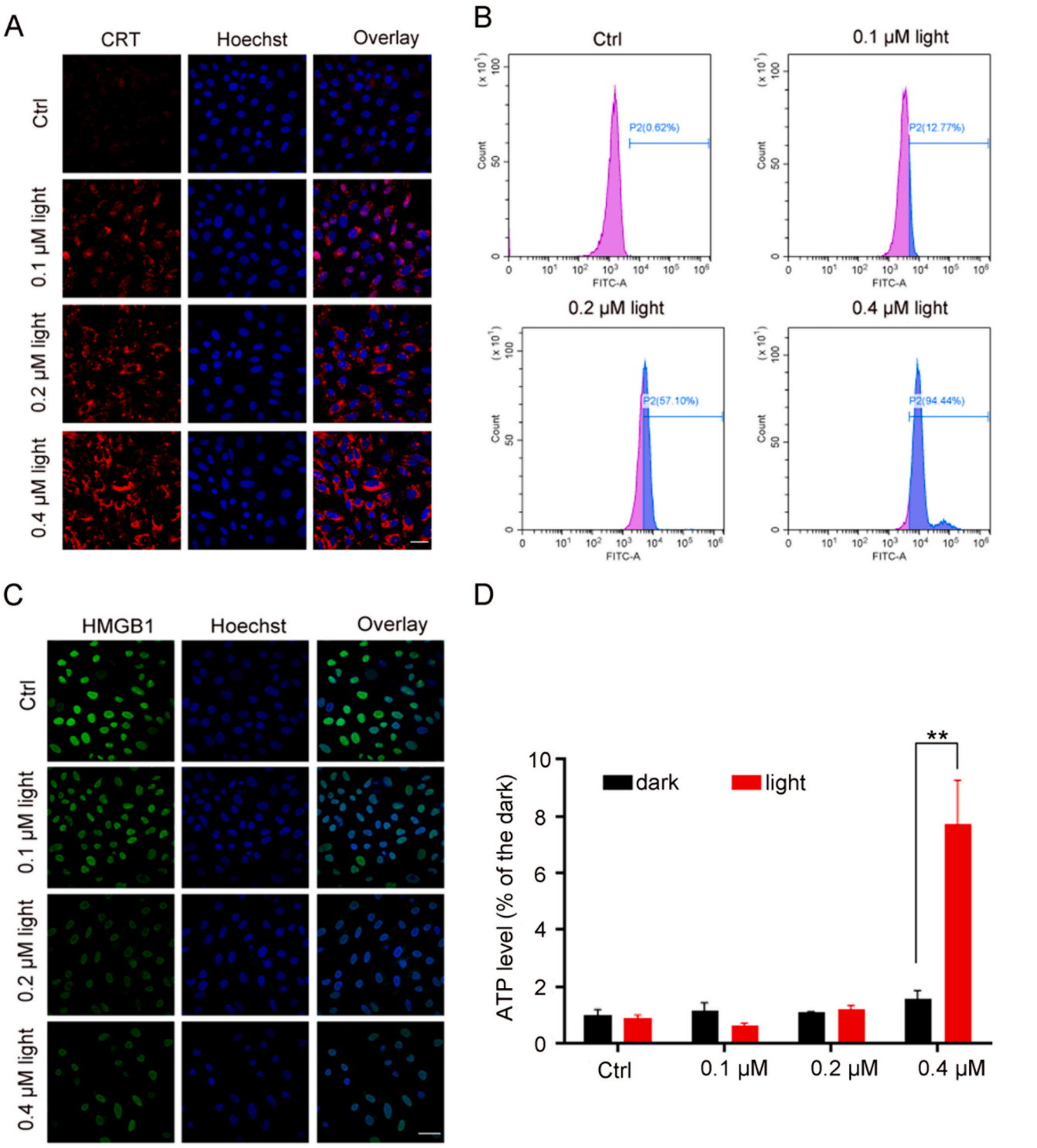

Fig. 6. (A) CLSM images and (B) flow cytometry analysis of ecto-CRT in MDA-MB-231 cells treated with **Ir3** (0 μM, 0.1 μM, 0.2 μM, and 0.4 μM) + PDT (15 mW/cm^2, 15 min). Scale bar: 20 μm. ecto-CRT: E_x = 633 nm, E_m = 650 ± 30 nm; Hoechst 33342: E_x = 405 nm, E_m = 430 ± 20 nm. (C) CLSM images of HMGB1 in MDA-MB-231 cells treated with **Ir3** (0 μM, 0.1 μM, 0.2 μM, and 0.4 μM) + PDT (15 mW/cm^2, 15 min). Scale bar: 20 μm. HMGB1: E_x = 488 nm, E_m = 520 ± 20 nm; Hoechst 33342: E_x = 405 nm, E_m = 430 ± 20 nm. (D) ATP levels in cell culture supernatants after **Ir3** and PDT treatment (425 nm, 15 mW/cm^2, 10 min). *$p < 0.05$, **$p < 0.01$, ***$p < 0.001$.

the ER and generates an immunomodulatory response through ICD. This is a promising photodynamic immunotherapy strategy.

CRediT authorship contribution statement

Yun-Shi Zhi: Writing – original draft, Investigation, Formal analysis. **Tie Chen:** Writing – original draft, Investigation, Formal analysis. **Bin-Fa Liang:** Investigation. **Shan Jiang:** Investigation. **Da-Hong Yao:** Resources. **Zhen-Dan He:** Resources. **Chen-Yang Li:** Resources, Funding acquisition. **Liang He:** Writing – review & editing, Resources, Funding acquisition. **Zheng-Yin Pan:** Writing – review & editing, Supervision, Funding acquisition, Conceptualization.

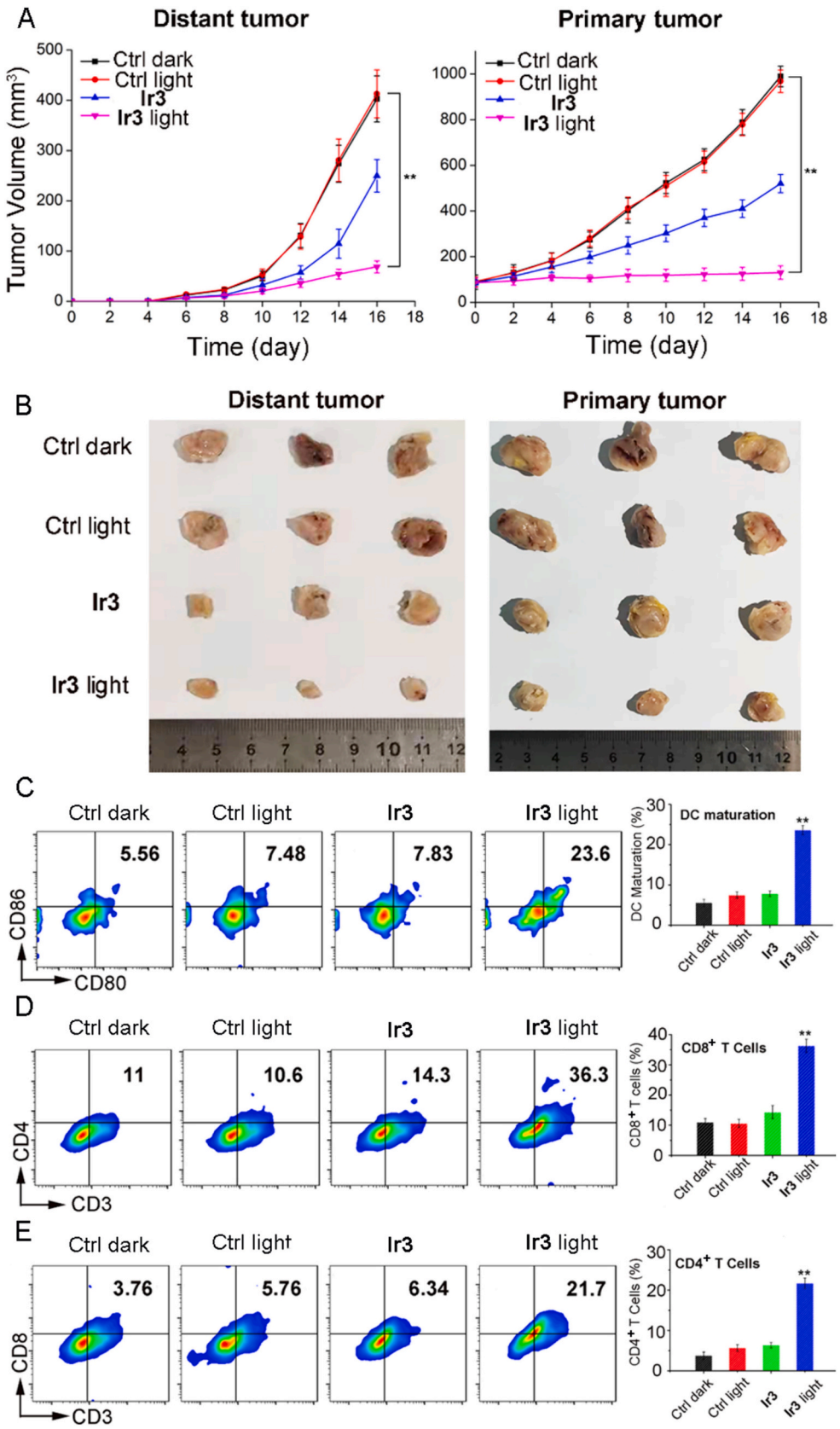

Fig. 7. *In vivo* anti-tumor efficacy and anti-tumor immune response. (A) Volume changes of primary and distant tumors: (black dot) Ctrl + dark, (red dot) Ctrl + light, (blue dot) **Ir3**, (pink dot) **Ir3** + light, ($n = 3$). (B) The photographs of the tumor collected at the end of the therapeutic period. *In vivo* anti-tumor immune response. (C) Expression of CD 80+ and CD 86+ quantitatively detected by flow cytometry *in vivo* (n = 3). (D-E) Populations of CD4+ and CD8+ T cells in distant tumors (n = 3). *$p < 0.05$, **$p < 0.01$, ***$p < 0.001$, by Student's two-tailed *t*-test. (For interpretation of the references to colour in this figure legend, the reader is referred to the web version of this article.)

Declaration of competing interest

The authors declare that they have no known competing financial interests or personal relationships that could have appeared to influence the work reported in this paper.

Data availability

Data will be made available on request.

Acknowledgements

This work was supported by National Natural Science Foundation of China (22107074), Guangdong Basic and Applied Basic Research Foundation (2024A1515030157, 2022A1515011356, 2021A1515110211), Shenzhen Natural Science Fund (the Stable Support Plan Program 20220811110339002), the Shenzhen Science and Technology Innovation Program (JCYJ20230808105913028), Shenzhen Longgang District Science and Technology Innovation Bureau (LGKCYLWS2021000001).

Appendix A. Supplementary data

Supplementary data to this article can be found online at https://doi.org/10.1016/j.jinorgbio.2024.112695.

References

[1] A.K. Palucka, L.M. Coussens, The basis of Oncoimmunology, Cell 164 (6) (2016) 1233–1247.
[2] I. Mellman, G. Coukos, G. Dranoff, Cancer immunotherapy comes of age, Nature 480 (7378) (2011) 480–489.
[3] G.K. Pennock, L.Q. Chow, The evolving role of immune checkpoint inhibitors in Cancer treatment, Oncologist 20 (7) (2015) 812–822.
[4] J. Ma, L. Huang, D. Hu, S. Zeng, Y. Han, H. Shen, The role of the tumor microbe microenvironment in the tumor immune microenvironment: bystander, activator, or inhibitor? J. Exp. Clin. Cancer Res. 40 (1) (2021) 327, https://doi.org/10.1186/s13046-021-02128-w.
[5] D. Hanahan, R.A. Weinberg, Hallmarks of cancer: the next generation, Cell 144 (5) (2011) 646–674.
[6] X. Lei, Y. Lei, J.K. Li, W.X. Du, R.G. Li, J. Yang, J. Li, F. Li, H.B. Tan, Immune cells within the tumor microenvironment: biological functions and roles in cancer immunotherapy, Cancer Lett. 470 (2020) 126–133.
[7] S. Zhang, J. Wang, Z. Kong, X. Sun, Z. He, B. Sun, C. Luo, J. Sun, Emerging photodynamic nanotherapeutics for inducing immunogenic cell death and potentiating cancer immunotherapy, Biomaterials 282 (2022) 121433, https://doi.org/10.1016/j.biomaterials.2022.121433.
[8] S. Zhang, Z. Wang, Z. Kong, Y. Wang, X. Zhang, B. Sun, H. Zhang, Q. Kan, Z. He, C. Luo, J. Sun, Photosensitizer-driven nanoassemblies of homodimeric prodrug for self-enhancing activation and synergistic chemo-photodynamic therapy, Theranostics 11 (12) (2021) 6019–6032.
[9] N. Yang, W. Xiao, X. Song, W. Wang, X. Dong, Recent advances in tumor microenvironment hydrogen peroxide-responsive materials for Cancer photodynamic therapy, Nano Lett. 12 (1) (2020) 15, https://doi.org/10.1007/s40820-019-0347-0.
[10] S. Zhang, Y. Wang, Z. Kong, X. Zhang, B. Sun, H. Yu, Q. Chen, C. Luo, J. Sun, Z. He, Pure photosensitizer-driven nanoassembly with core-matched PEGylation for imaging-guided photodynamic therapy, Acta Pharm. Sin. B 11 (11) (2021) 3636–3647.
[11] E. Panzarini, V. Inguscio, G.M. Fimia, L. Dini, Rose Bengal acetate photodynamic therapy (RBAc-PDT) induces exposure and release of damage-associated molecular patterns (DAMPs) in human HeLa cells, PLoS One 9 (8) (2014) 105778.
[12] W. Li, J. Yang, L. Luo, M. Jiang, B. Qin, H. Yin, C. Zhu, X. Yuan, J. Zhang, Z. Luo, Y. Du, Q. Li, Y. Lou, Y. Qiu, J. You, Targeting photodynamic and photothermal therapy to the endoplasmic reticulum enhances immunogenic cancer cell death, Nat. Commun. 10 (1) (2019) 3349, https://doi.org/10.1038/s41467-019-11269-8.
[13] Y. Li, X. Liu, W. Pan, N. Li, B. Tang, Photothermal therapy-induced immunogenic cell death based on natural melanin nanoparticles against breast cancer, Chem. Commun. 56 (9) (2020) 1389–1392.
[14] K.B. Huang, F.Y. Wang, H.W. Feng, H. Luo, Y. Long, T. Zou, A.S.C. Chan, R. Liu, H. Zou, Z.F. Chen, Y.C. Liu, Y.N. Liu, H. Liang, An aminophosphonate ester ligand-containing platinum(ii) complex induces potent immunogenic cell death in vitro and elicits effective anti-tumour immune responses in vivo, Chem. Commun. 55 (87) (2019) 13066–13069.
[15] L. Wang, R. Guan, L. Xie, X. Liao, K. Xiong, T.W. Rees, Y. Chen, L. Ji, H. Chao, An ER-targeting iridium(III) complex that induces immunogenic cell death in non-small-cell lung Cancer, Angew. Chem. Int. Ed. 60 (9) (2021) 4657–4665.
[16] P. Broz, P. Pelegrin, F. Shao, The gasdermins, a protein family executing cell death and inflammation, Nat. Rev. Immunol. 20 (3) (2020) 143–157.
[17] X. Liu, Z. Zhang, J. Ruan, Y. Pan, V.G. Magupalli, H. Wu, J. Lieberman, Inflammasome-activated gasdermin D causes pyroptosis by forming membrane pores, Nature 535 (7610) (2016) 153–158.
[18] Y. Wang, W. Gao, X. Shi, J. Ding, W. Liu, H. He, K. Wang, F. Shao, Chemotherapy drugs induce pyroptosis through caspase-3 cleavage of a gasdermin, Nature 547 (7661) (2017) 99–103.
[19] C. Rogers, T. Fernandes-Alnemri, L. Mayes, D. Alnemri, G. Cingolani, E.S. Alnemri, Cleavage of DFNA5 by caspase-3 during apoptosis mediates progression to secondary necrotic/pyroptotic cell death, Nat. Commun. 8 (2017) 14128.
[20] H. Lu, S. Zhang, J. Wu, M. Chen, M.C. Cai, Y. Fu, W. Li, J. Wang, X. Zhao, Z. Yu, P. Ma, G. Zhuang, Molecular targeted therapies elicit concurrent apoptotic and GSDME-dependent Pyroptotic tumor cell death, Clin. Cancer Res. 24 (23) (2018) 6066–6077.
[21] T. Du, J. Gao, P. Li, Y. Wang, Q. Qi, X. Liu, J. Li, C. Wang, L. Du, Pyroptosis, metabolism, and tumor immune microenvironment, Clin. Transl. Med. 11 (8) (2021) 492, https://doi.org/10.1002/ctm2.492.
[22] R. Guan, Y. Chen, L. Zeng, T.W. Rees, C. Jin, J. Huang, Z.S. Chen, L. Ji, H. Chao, Oncosis-inducing cyclometalated iridium(iii) complexes, Chem. Sci. 9 (23) (2018) 5183–5190.
[23] H. Yuan, Z. Han, Y. Chen, F. Qi, H. Fang, Z. Guo, S. Zhang, W. He, Ferroptosis Photoinduced by new Cyclometalated iridium(III) complexes and its synergism with apoptosis in tumor cell inhibition, Angew. Chem. Int. Ed. 60 (15) (2021) 8174–8181.
[24] W. Lin, Y. Liu, J. Wang, Z. Zhao, K. Lu, H. Meng, R. Luoliu, X. He, J. Shen, Z. W. Mao, W. Xia, Engineered Bacteria labeled with iridium(III) photosensitizers for enhanced photodynamic immunotherapy of solid tumors, Angew. Chem. Int. Ed. 62 (43) (2023) e202310158, https://doi.org/10.1002/anie.202310158.
[25] M.M. Wang, F.J. Xu, Y.Y. Su, X.T. Geng, X.L. Qian, Y.Q. Xue, Z.H. Yu Kong, H. K. Liu, Z. Su, A new strategy to fight Metallodrug resistance: mitochondria-relevant treatment through Mitophagy to inhibit metabolic adaptations of Cancer cells, Angew. Chem. Int. Ed. 61 (27) (2022), https://doi.org/10.1002/anie.202203843 e202203843.
[26] W.J. Wang, Y.-Y. Ling, Y.-M. Zhong, Z.-Y. Li, C.P. Tan, Z.W. Mao, Ferroptosis-enhanced Cancer immunity by a ferrocene-appended iridium(III) Diphosphine complex, Angew. Chem. Int. Ed. 61 (16) (2022), https://doi.org/10.1002/ange.202115247 e202115247.
[27] S. Kuang, X. Liao, X. Zhang, T.W. Rees, R. Guan, K. Xiong, Y. Chen, L. Ji, H. Chao, FerriIridium: a lysosome-targeting Iron(III)-activated iridium(III) prodrug for chemotherapy in gastric Cancer cells, Angew. Chem. Int. Ed. 59 (8) (2020) 3315–3321.
[28] M. Lv, Y. Zheng, J. Wu, Z. Shen, B. Guo, G. Hu, Y. Huang, J. Zhao, Y. Qian, Z. Su, C. Wu, X. Xue, H.K. Liu, Z.W. Mao, Evoking Ferroptosis by synergistic enhancement of a cyclopentadienyl iridium-Betulin immune agonist, Angew. Chem. Int. Ed. 62 (48) (2023) e202312897, https://doi.org/10.1002/anie.202312897.
[29] L. Wang, J. Karges, F. Wei, L. Xie, Z. Chen, G. Gasser, L. Ji, H. Chao, Mitochondria-localized iridium(iii) photosensitizer for two-photon photodynamic immunotherapy against melanoma, Chem. Sci. 14 (6) (2023) 1461–1471.
[30] J.Y. Zhou, Q.H. Shen, X.J. Hong, W.Y. Zhang, Q. Su, W.G. Li, B. Cheng, C.P. Tan, T. Wu, Synergization of an endoplasmic reticulum-targeted iridium(III) photosensitizer with PD-L1 inhibitor for oral squamous cell carcinoma immunotherapy, Chem. Eng. J. 474 (2023) 145516.
[31] C. Gonzalo-Navarro, E. Zafon, J.A. Organero, F.A. Jalón, J.C. Lima, G. Espino, A. M. Rodríguez, L. Santos, A.J. Moro, S. Barrabés, J. Castro, J. Camacho-Aguayo, A. Massaguer, B.R. Manzano, G. Durá, Ir(III) half-Sandwich photosensitizers with a π-expansive ligand for efficient anticancer photodynamic therapy, J. Med. Chem. 67 (3) (2024) 1783–1811.
[32] Y. Wu, S. Huang, J. Wang, L. Sun, F. Zeng, S. Wu, Activatable probes for diagnosing and positioning liver injury and metastatic tumors by multispectral optoacoustic tomography, Nat. Commun. 9 (1) (2018) 3983, https://doi.org/10.1038/s41467-018-06499-1.
[33] M. Watanabe, S.M. Houten, C. Mataki, M.A. Christoffolete, B.W. Kim, H. Sato, N. Messaddeq, J.W. Harney, O. Ezaki, T. Kodama, K. Schoonjans, A.C. Bianco, J. Auwerx, Bile acids induce energy expenditure by promoting intracellular thyroid hormone activation, Nature 439 (7075) (2006) 484–489.
[34] G.A. Kullak-Ublick, B. Stieger, P.J. Meier, Enterohepatic bile salt transporters in normal physiology and liver disease, Gastroenterology 126 (1) (2004) 322–342.
[35] Y. Zhang, X. Chen, Q. Yuan, Y. Bian, M. Li, Y. Wang, X. Gao, D. Su, Enzyme-activated near-infrared fluorogenic probe with high-efficiency intrahepatic targeting ability for visualization of drug-induced liver injury, Chem. Sci. 12 (44) (2021) 14855–14862.
[36] H.G. Xu, M. Schikora, M. Sisa, S. Daum, I. Klemt, C. Janko, C. Alexiou, G. Bila, R. Bilyy, W. Gong, M. Schmitt, L. Sellner, A. Mokhir, An endoplasmic reticulum specific pro-amplifier of reactive oxygen species in Cancer cells, Angew. Chem. Int. Ed. 60 (20) (2021) 11158–11162.
[37] X. Xu, M. Chen, S. Jiang, Z. Pan, C. Zhao, Endoplasmic reticulum-targeting iridium (III) Nanosonosensitizer amplifies immunogenic cell death for boosted tumor Sono-immunotherapy, Adv. Funct. Mater. 2314780 (2024).
[38] Y. Su, J. Yang, M.M. Wang, H.-B. Fang, H.K. Liu, Z.H. Yu, Z. Su, Cyclometalated iridium(III) complexes as anti-breast cancer and anti-metastasis agents via STAT3 inhibition, J. Inorg. Biochem. 251 (2024) 112427.
[39] W. Hu, R. Liu, K. Zheng, Z. Wang, Highly photoactive Ir(iii)–Pt(iv) heterometallic conjugates for anticancer therapy, Chem. Commun. 60 (4) (2024) 388–391.
[40] O.B. Ijare, B.S. Somashekar, Y. Jadegoud, G.A. Nagana Gowda, 1H and 13C NMR characterization and stereochemical assignments of bile acids in aqueous media, Lipids 40 (10) (2005) 1031.

[41] W.W. Qin, Z.Y. Pan, D.H. Cai, Y. Li, L. He, Cyclometalated iridium(iii) complexes for mitochondria-targeted combined chemo-photodynamic therapy, Dalton Trans. 49 (11) (2020) 3562–3569.
[42] Y. Rong, Z. Fan, Z. Yu, L. Wei, H. Shen, H. Huang, X. Hao, Z. Zhao, J. Wang, An endoplasmic reticulum-targeting iridium(iii) complex induces immunogenic cell death in melanoma cells and enhances anti-PD-1 immunotherapy by remodeling tumor microenvironment, Inorg. Chem. Front. 10 (18) (2023) 5278–5291.
[43] L. Zhou, F. Wei, J. Xiang, H. Li, C. Li, P. Zhang, C. Liu, P. Gong, L. Cai, K.M.-C. Wong, Enhancing the ROS generation ability of a rhodamine-decorated iridium (iii) complex by ligand regulation for endoplasmic reticulum-targeted photodynamic therapy, Chem. Sci. 11 (44) (2020) 12212–12220.
[44] X. Li, Z. Wang, X. Hao, J. Zhang, X. Zhao, Y. Yao, W. Wei, R. Cai, C. He, C. Duan, Z. Guo, J. Zhao, X. Wang, Optically pure double-stranded Dinuclear Ir(III) Metallohelices enabled chirality-induced photodynamic responses, J. Am. Chem. Soc. 145 (27) (2023) 14766–14775.
[45] E. Bobrovnikova-Marjon, C. Grigoriadou, D. Pytel, F. Zhang, J. Ye, C. Koumenis, D. Cavener, J.A. Diehl, PERK promotes cancer cell proliferation and tumor growth by limiting oxidative DNA damage, Oncogene 29 (27) (2010) 3881–3895.
[46] J. Ye, R.B. Rawson, R. Komuro, X. Chen, U.P. Dave, R. Prywes, M.S. Brown, J. L. Goldstein, ER stress induces cleavage of membrane-bound ATF6 by the same proteases that process SREBPs, Mol. Cell 6 (6) (2000) 1355–1364.
[47] J. Wu, D.T. Rutkowski, M. Dubois, J. Swathirajan, T. Saunders, J. Wang, B. Song, G.D. Yau, R.J. Kaufman, ATF6alpha optimizes long-term endoplasmic reticulum function to protect cells from chronic stress, Dev. Cell 13 (3) (2007) 351–364.
[48] J. Tao, H. Chen, X. Li, J. Wang, The role of activating transcription factor 6 in hydroxycamptothecin-induced fibroblast autophagy and apoptosis, J. Orthop. Surg. Res. 16 (1) (2021) 1, https://doi.org/10.1186/s13018-020-02056-z.
[49] T. Kong, Z. He, S. Wang, C. Jiang, F. Zhu, J. Gao, L. Li, Y. Wang, Q. Xie, Y. Li, Diterpenoid DGA induces apoptosis via endoplasmic reticulum stress caused by changes in glycosphingolipid composition and inhibition of STAT3 in glioma cells, Biochem. Pharmacol. 205 (2022) 115254, https://doi.org/10.1016/j.bcp.2022.115254.
[50] M. Song, C. Wang, H. Yang, Y. Chen, X. Feng, B. Li, H. Fan, P-STAT3 inhibition activates endoplasmic reticulum stress-induced Splenocyte apoptosis in chronic stress, Front. Physiol. 11 (2020) 680.
[51] R. Hu, Q. Han, J. Zhang, STAT3: a key signaling molecule for converting cold to hot tumors, Cancer Lett. 489 (2020) 29–40.